García-Pozuelo, D., Olatunbosun, O., Romano, L., Strano, S., Terzo, M., Tuononen, A.J., Xiong, Y. (2019). Development and experimental validation of a real-time analytical model for different intelligent tire concepts. *Vehicle System Dynamics*, v. 57.

DOI: https://doi.org/10.1080/00423114.2019.1566560

Development and experimental validation of a real-time analytical model for different intelligent tire concepts

Daniel Garcia-Pozuelo[1], Oluremi Olatunbosun[2], Luigi Romano[3], Salvatore Strano[3*], Mario Terzo[3], Ari J. Tuononen[4], Yi Xiong[5]

[1]*Mechanical Engineering Department, Universidad Carlos III de Madrid, Avd. De la Universidad, 28911 Madrid, Spain.*

[2] *School of Mechanical Engineering, University of Birmingham, Edgbaston B15 2TT, UK.*

[3]*Department of Industrial Engineering, University of Naples Federico II, 80125 Naples, Italy.*

[4] *Department of Mechanical Engineering, Aalto University, Espoo, Finland.*

[5] *Digital Design and Manufacturing Center, Singapore University of Technology and Design Singapore, Singapore.*

Abstract

In recent years, the ever-increasing interest in intelligent tire technology has led to the formulation of different empirical models correlating deformation measurements provided by the sensors with tire dynamics.

In this paper, a real-time physical model, suitable for describing the dynamics of intelligent tires based on measurements of strains and/or displacements of the tire carcass, is presented. The proposed flexible ring model can reproduce the tire dynamics for both concentrated and distributed forces by introducing a discrete approach that also allows to analyse the longitudinal dynamics of the tire in real-time.

The analytical description of the problem allows to obtain solutions in closed form and to quickly identify model parameters from experimental data. The comparison between the simulated results and the ones provided by indoor tests of two intelligent tire concepts highlighted that the proposed tire model can estimate with an acceptable precision both the carcass deformations and the forces acting on the tire.

keywords: intelligent tire; flexible ring model; real-time tire model; analytical modelling.

1. Introduction

A great deal of research has been directed towards the development of intelligent tires since the early 90s. Nowadays, the constant evolution of the automotive sector and the ever increasing need to optimise the performances of both commercial and sport vehicles is progressively involving the use of embedded systems in a complex multifunctional environment. It is well known that the tires represent the only component of a vehicle able to exchange traction forces with the environment, and sensors installed in their inner-liner could be able to provide useful information about tire and road conditions. Consequently, a more reliable knowledge of tire-road interaction provided by an integrated sensory system could improve driving safety and vehicle dynamics performances. In [1], an extensive review of technologies and estimation methods for intelligent tire systems has been presented. Many research applications concerning intelligent tires adopt sensors installed on the inner liner and are divided into acceleration-based [2-5] and strain-based [6-15]. Other measurement systems are also presented in literature with interesting results. For instance, Magori *et al.* [16] installed an ultrasonic sensor on the base of a wheel rim to monitor the deformation, temperature, and other contact patch features. Tuononen [17, 18] has carried out several studies to measure tire carcass deflections by means of an optical sensor to provide estimations about the vehicle state. A segmented capacitance ring sensor for measuring the inflation pressure of the tire has been presented in [19].

A highly demanding topic for the above-mentioned intelligent tire concepts is the development of algorithms for the analysis of the sensor data. Generally, correlations between sensor measurements and tire operative conditions are based on signal processing techniques that are time-consuming due to extensive experimental tests and the large amount of data to be analysed [1].

Within this context, a model-based approach for estimation of the main dynamical characteristics of intelligent tires could be extremely useful. For this purpose, a physical tire model is presented in this paper with the main objective of being applicable to different types of tires. Many of the conventional tire models are not suitable for modelling intelligent tires because they provide as output forces starting from longitudinal and lateral slips, frictions, etc., without information concerning local deformations or accelerations of the pneumatic tire [20-22]. Finite element models could provide complete and precise dynamical responses, but they are not suitable for real-time

applications due to their computational loads [23, 25]. A simplified tire model for intelligent tires is presented in [26].

The analytical tire model presented in this paper can predict, in real-time, the structural behaviour of the tire carcass according to the driving conditions. In particular, the physical modelling approach is based on the tire model developed by Gong [27, 28], which has been adapted to provide an analytical solution for the radial and tangential displacements of the tread in real-time. The tire-road contact problem has also been modelled by means of a simplified approach that consists in imposing a parabolic normal pressure distribution. In this way, the solutions for both the radial and tangential displacements can be obtained in closed-form, further reducing the computational effort.

The model has been validated through experimental data from two types of intelligent tires to highlight the modelling versatility. More specifically, experimental data from [17, 29] and [30] have been achieved for the model parameterization and validation.

This paper is organized as follows: in section 2, the modelling approach is illustrated; simulation results are presented in section 3; the experimental validation is described in section 4 and conclusions and future developments are drawn in section 5.

2. Tire mathematical model

The flexible ring tire models (FRTMs) have been developed in the early 60s to study the deformation of the tire carcass in stationary conditions; some more recent efforts have also been made to simulate the behaviour of the tire on uneven roads [31] - [32]. Depending on the underlying assumptions, these models provide accurate results in different frequency ranges.

The well-known FRTM developed by Gong [27] has been extensively used to investigate the natural frequencies of the tire and to study the problems of vibration transmission in a wide frequency range (0-300 Hz); however, its ability to provide a closed form solution for the trend of the circumferential strain also makes it suitable to study the deformation of the tire carcass. The main drawback of the model is that the equations of the deformation are coupled with those of the motion. In contrast, some newer models [32] do not provide results on the circumferential strain of the tyre carcass directly, but they make use of simplifying hypotheses that allow decoupling of the two problems, and perhaps could even be better suited for real-time applications; in particular, the model developed by Kim *et al* [32] seems capable of predicting the deformation of the treadband

with great accuracy and at a low computational cost. Hence, it could be eventually adapted employing the usual plane-strain relations for curved beams.

Therefore, the comparison between the two approaches could be presented in a further research paper.

In this study, the deformation of the tire carcass due to applied steady-state forces is investigated only with Gong's FRTM to obtain a closed-form solution for the tire deflection problem; furthermore, the solutions for the ring displacements provided by employing the *Modal Expansion Method* (MEM) are further simplified introducing a discrete approach which streamlines the model from a computational standpoint and allows the simulation of the tire behaviour in real-time.

In the FRTM, the treadband structure is modelled as homogeneous, thin circular elastic ring restrained at its inner surface both in circumferential and radial directions by a viscoelastic foundation (Fig. 1a). This is schematically represented by spring and damper elements in the radial and tangential directions and takes into account the stiffness of the sidewall structure and the membrane stiffness of the inflated torus enclosed by the carcass. For the sake of simplicity, the damping and stiffness values are reported as their mean values, although some authors have shown that they are variable within the contact patch [33].

The location of an infinitesimal element of the ring is described in terms of cylindrical coordinates (R, ϕ) in the non-rotating coordinate system (x, z) (Fig. 1b).

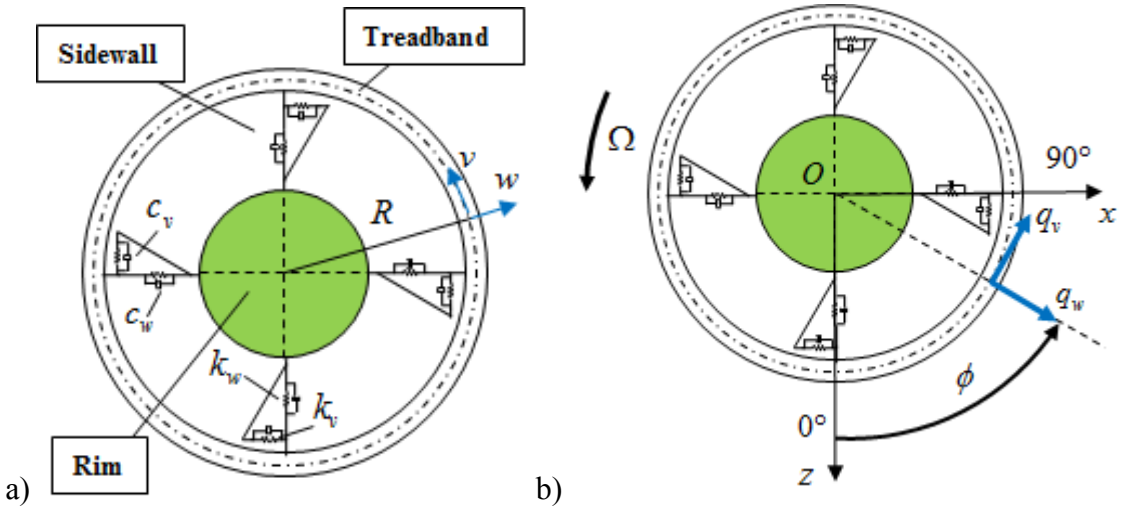

Fig. 1. a) The flexible ring model; b) Coordinate system.

In Fig. 1b, q_v, q_w and are the external forces in the tangential and radial directions, respectively. Because of the high extensional stiffness of the modern radial tire, the middle surface of the tire

carcass is assumed to be inextensible. Furthermore, according to the Bernoulli-Euler assumption, the treadband has been assumed as an inextensible, curved, bending beam. Under this hypothesis, the radial displacement *w* and tangential displacement *v* are governed by the following relation:

$$w = -\frac{\partial v}{\partial \phi}. \tag{1}$$

The circumferential strain also reads [27]:

$$\varepsilon_\theta = -\frac{y}{R^2}\left(\frac{\partial v}{\partial \theta} - \frac{\partial^2 w}{\partial \theta^2}\right) \tag{2}$$

2.1. Response to concentrated loads

In this paragraph, the response of the FRTM to concentrated line forces is described [28]. Consider the external line forces on the ring are expressed as

$$\begin{aligned} q_w(\theta,t) &= Q_w \delta(\phi - \phi_0) \\ q_v(\theta,t) &= Q_v \delta(\phi - \phi_0) \end{aligned} \tag{3}$$

where Q_w and Q_v are the magnitudes of radial and tangential line forces acting at specified stationary angular coordinate ϕ_0, respectively; $\delta(\cdot)$ is a Dirac delta function.

According to the MEM [27, 28], the steady state response of the FRTM in terms of the tangential displacement and the corresponding radial displacement of the tire treadband for the concentrated line forces are given by [28]:

$$v(\phi) = \sum_{n=0}^{\infty}\left[A_{n1}Q_v \cos n(\phi_0 - \phi + \gamma_n) + A_{n2}Q_w \sin n(\phi_0 - \phi + \gamma_n)\right] \tag{4}$$

With:

$$
\begin{aligned}
A_{n1} &= \frac{1}{\pi\sqrt{\left(M_n - G_n\right)^2 + \left(C_n\right)^2}} \\
A_{n2} &= nA_{n1} \\
n\gamma_n &= \tan^{-1}\left(\frac{C_n}{M_n - G_n}\right) \\
M_n &= k_n - \left(n\Omega\right)^2 m_n \\
G_n &= \left(n\Omega\right)g_n \\
C_n &= \left(n\Omega\right)c_n \\
m_n &= \rho A\left(1+n^2\right) \\
g_n &= -4\rho A n\Omega \\
c_n &= c_v + c_w n^2 \\
k_n &= \left(\frac{EI}{R^4}n^2 + \frac{\sigma_\theta^0}{R^2}\right)\left(1-n^2\right)^2 - \frac{p_0 b}{R}\left(1-n^2\right) + k_v + k_w n^2 - \rho A\left(1+n^2\right)\Omega^2 \\
\sigma_\theta^0 A &= \left(p_0 bR + \rho A R^2\Omega^2\right)
\end{aligned}
\tag{5}
$$

2.2. Response to distributed loads in the contact patch

Consider a distributed load extending from the angular coordinate ϕ_f at the front edge of the contact patch to ϕ_r at the rear edge is applied to the tire. By adopting the MEM, the tangential and radial displacements are given by:

$$
\begin{aligned}
v(\phi) &= \sum_{n=1}^{\infty}\left[\left(\alpha_{n1}A_{n1} - \alpha_{n3}A_{n2}\right)\sin\left(n\left(\phi-\gamma_n\right)\right) + \left(\alpha_{n2}A_{n1} + \alpha_{n4}A_{n2}\right)\cos\left(n\left(\phi-\gamma_n\right)\right)\right] \\
w(\phi) &= \sum_{n=1}^{\infty} n\left[\left(\alpha_{n3}A_{n2} - \alpha_{n1}A_{n1}\right)\cos\left(n\left(\phi-\gamma_n\right)\right) + \left(\alpha_{n2}A_{n1} + \alpha_{n4}A_{n2}\right)\sin\left(n\left(\phi-\gamma_n\right)\right)\right]
\end{aligned}
\tag{6}
$$

where:

$$\alpha_{n1} = \int_{\phi_f}^{\phi_r} q_v(\phi)\sin(n\phi)d\phi$$
$$\alpha_{n2} = \int_{\phi_f}^{\phi_r} q_v(\phi)\cos(n\phi)d\phi$$
$$\alpha_{n3} = \int_{\phi_f}^{\phi_r} q_w(\phi)\cos(n\phi)d\phi \quad . \qquad (7\ a,b,c,d)$$
$$\alpha_{n4} = \int_{\phi_f}^{\phi_r} q_w(\phi)\sin(n\phi)d\phi$$

2.2.1. Normal and tangential tire/road interactions

The previous analysis followed that one presented in [27]. However, to streamline the model from a computational point of view, here the normal pressure distribution, acting on the contact patch of the tire and related to the vertical load F_z, is approximated with a parabolic trend [12]. In particular, the pressure distribution is assigned as a function of the angular coordinate as follows:

$$q_z(\phi) = \frac{3}{4}\frac{F_z}{R\phi_r^3}\left(\phi_r^2 - \phi^2\right), \qquad (8)$$

where the symmetrical condition $\phi_r = -\phi_f$ is considered.

The corresponding radial pressure distribution can be obtained as:

$$q_w^{NI}(\phi) = \frac{3}{4}\frac{F_z}{R\phi_r^3}\left(\phi_r^2 - \phi^2\right)\cdot\frac{1}{\cos(\phi)} \qquad (9)$$

where the apex NI denotes the pressure contribution due to the normal interaction.

The FRTM can also provide the solution for the tangential interaction problem. In this paper, the tangential interaction of the rolling tire with the road is modelled with a brush model. Introducing the slip ratio ε_x, the tangential stiffness of the bristle k_x and assuming a generalized Coulomb friction model, the tangential force per unit of length is given by:

$$\tau_x(\phi) = \begin{cases} (\phi_f - \phi)k_x\varepsilon_x, & (\phi_f - \phi)k_x\varepsilon_x \le \mu_s q_z(\phi) \\ -\mu_d q_z(\phi)\,\mathrm{sgn}(\varepsilon_x), & \text{elsewhere} \end{cases} \qquad (10)$$

whose components in radial and tangential direction are, respectively:

$$\begin{aligned} q_w^{TI}(\phi) &= \tau_x(\phi)\sin(\phi) \\ q_v^{TI}(\phi) &= \tau_x(\phi)\cos(\phi) \end{aligned}, \tag{11}$$

where μ_s and μ_d are the static and dynamic friction coefficients, respectively, and the apex TI denotes the radial and tangential pressure contributions due to the longitudinal load. The radial and the tangential forces per unit of length are:

$$\begin{aligned} q_w(\phi) &= q_w^{NI}(\phi) + q_w^{TI}(\phi) \\ q_v(\phi) &= q_v^{TI}(\phi) \end{aligned}, \tag{12}$$

substituting (9) in (12) it follows:

$$\begin{aligned} q_w(\phi) &= \frac{3}{4}\frac{F_z}{R\phi_r^3}\frac{\left(\phi_r^2 - \phi^2\right)}{\cos(\phi)} + \tau_x(\phi)\sin(\phi) \\ q_v(\phi) &= \tau_x(\phi)\cos(\phi) \end{aligned}. \tag{13}$$

2.2.2. Discrete approach

Substituting expressions of the distributed loads (13) in (7), the radial and tangential displacements can be obtained from (6). However, solving equations (7) and (6) in a closed form is cumbersome; therefore, a discrete approach to the problem is provided in this study. The solution for both the normal contact problem and the tangential one is then obtained by superimposing the solution for each concentrated load.

If the angular interval between the front and rear angles ϕ_f and ϕ_r is already known, it can be divided in N_ϕ constant angular steps $\Delta\phi$. So, the generic concentrated forces $Q_{w,i}$ and $Q_{v,i}$ acting at point $\phi_{0,i}$ can be written as:

$$\begin{aligned} Q_{w,i} &= q_w(\phi_{0,i})\Delta\phi \\ Q_{v,i} &= q_v(\phi_{0,i})\Delta\phi \end{aligned}. \tag{14}$$

Hence, the tangential and radial deformations can be obtained by superimposing the solution:

$$\begin{aligned} v(\phi) &= \sum_{i=1}^{N_\phi}\sum_{n=1}^{\infty}\left[A_{n1}Q_{v,i}\cos\left(n\left(\phi_{0,i} - \phi + \gamma_n\right)\right) + A_{n2}Q_{w,i}\sin\left(n\left(\phi_{0,i} - \phi + \gamma_n\right)\right)\right] \\ w(\phi) &= \sum_{i=1}^{N_\phi}\sum_{n=1}^{\infty} n\left[-A_{n1}Q_{v,i}\sin\left(n\left(\phi_{0,i} - \phi + \gamma_n\right)\right) + A_{n2}Q_{w,i}\cos\left(n\left(\phi_{0,i} - \phi + \gamma_n\right)\right)\right] \end{aligned}. \tag{15}$$

Substituting equations (15) into (2), the circumferential strain can be also obtained:

$$\varepsilon_\theta(\phi) = \sum_{i=1}^{n_i}\sum_{n=1}^{\infty}\frac{y}{R^2}n^3\left[A_{n1}Q_{v,i}\sin\left(n\left(\phi_{0,i}-\phi+\gamma_n\right)\right)-A_{n2}Q_{w,i}\cos\left(n\left(\phi_{0,i}-\phi+\gamma_n\right)\right)\right]. \quad (16)$$

The parameters of the FRTM are listed in Table 1.

Symbol	Description	Unit
b	Width of the ring.	m
h	Thickness of the ring.	m
A	Area of the cross section of the ring ($A=bh$).	m^2
E	Young's modulus of the ring material.	N/m^2
I	Inertia moment of the cross-section of the ring ($I=bh^3/12$).	m^4
R	Mean radius of the ring (tire treadband).	m
ρ	Density of the ring material.	kg/m^3
k_w, k_v	Stiffness of the viscoelastic foundation per unit length in the radial and tangential directions, respectively.	N/m^2
c_w, c_v	Damping of the viscoelastic foundation per unit length in the radial and tangential directions, respectively.	$N\ s/m^2$
k_x	Bristle tangential stiffness	N/m
ε_x	Slip ratio	-

Table 1. Parameters of the FRTM.

3. Simulation results

A first set of simulation has been performed to evaluate the qualitative trend of both displacements and strain by adopting parameters presented in [28] and listed in Table 2.

Parameters	Value	Unit
b	0.14	m
h	0.01	m
EI	2.0	Nm^2
R	0.3	m
ρA	3.15	kg/m
k_w	$6.3\cdot10^5$	N/m^2
k_v	$1.9\cdot10^5$	N/m^2

$c_w = c_v$	0	N s/m^2
k_x	$5.43 \cdot 10^5$	N/m
p_0	$1.2 \cdot 10^5$	N/m^2

Table 2. Values of the FRTM parameters used for simulations.

Fig. 2a and Fig. 2b show the behaviours of *w* and *v*, obtained with the distributed load approach, by varying the inflation pressure and the vertical load, respectively.

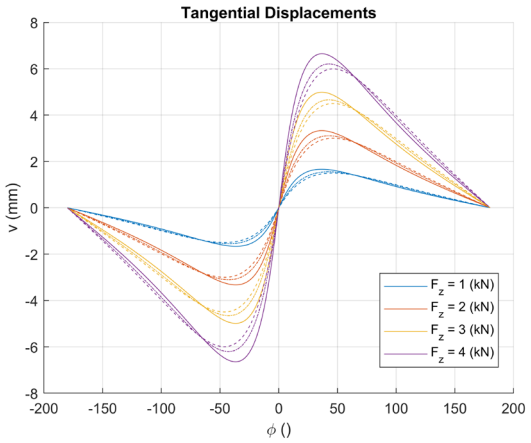

a)

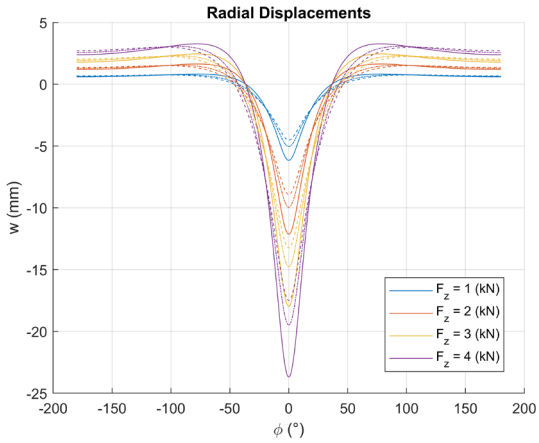

b)

Fig. 2. Displacements under different inflation pressures and vertical loads: a) *Tangential displacements*; b) *Radial displacements*; (solid: 1.2 bar, dashed: 2.0 bar, dash-dotted: 2.6 bar).

A further set of simulations has been performed to compare the radial and tangential deformations output from the two models (concentrated and distributed forces, respectively). Figs. 3a,b compare radial displacements for the concentrated force model (red) and distributed one (black) under vertical loads F_z = 500 N and F_z = 5000 N, respectively.

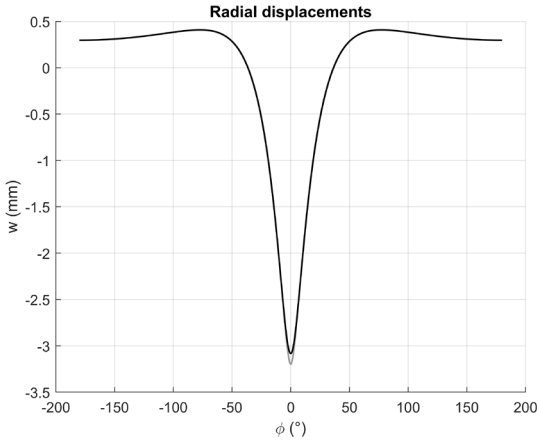

a)

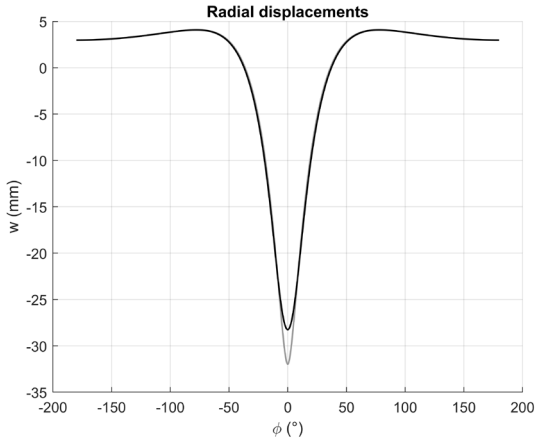

b)

Fig. 3. Radial displacements: a) F_z = 500 N; b) F_z = 5000 N.

Comparisons between tangential displacements for the concentrated force model (red) and distributed one (black), for vertical loads F_z = 500 N and F_z = 5000 N, are shown in Fig. 4a,b, respectively.

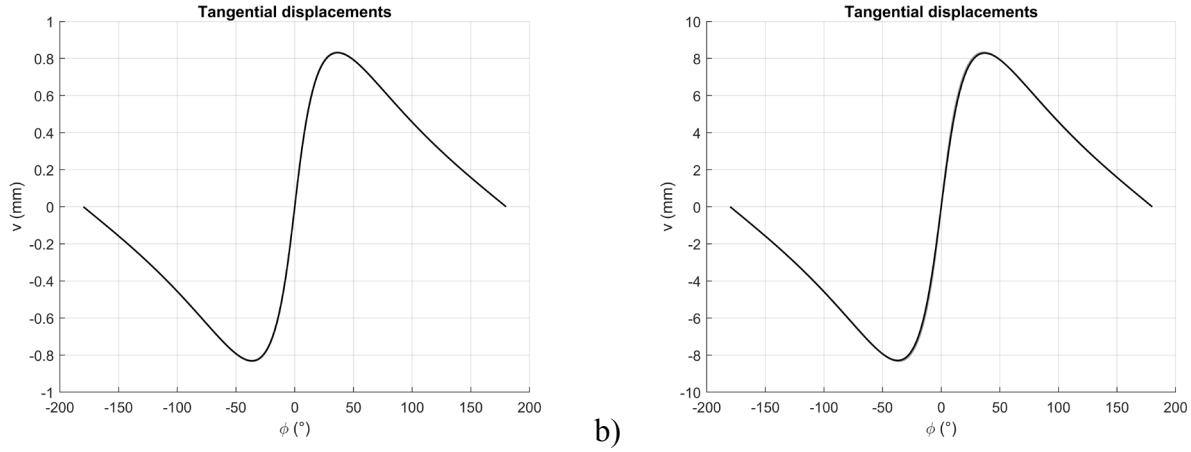

a) b)

Fig. 4. Tangential displacements: a) F_z = 500 N; b) F_z = 5000 N.

Figs. 5a,b present the simulated circumferential strains for the concentrated force model (red) and distributed one (black) under vertical loads F_z = 500 N and F_z = 5000 N, respectively.

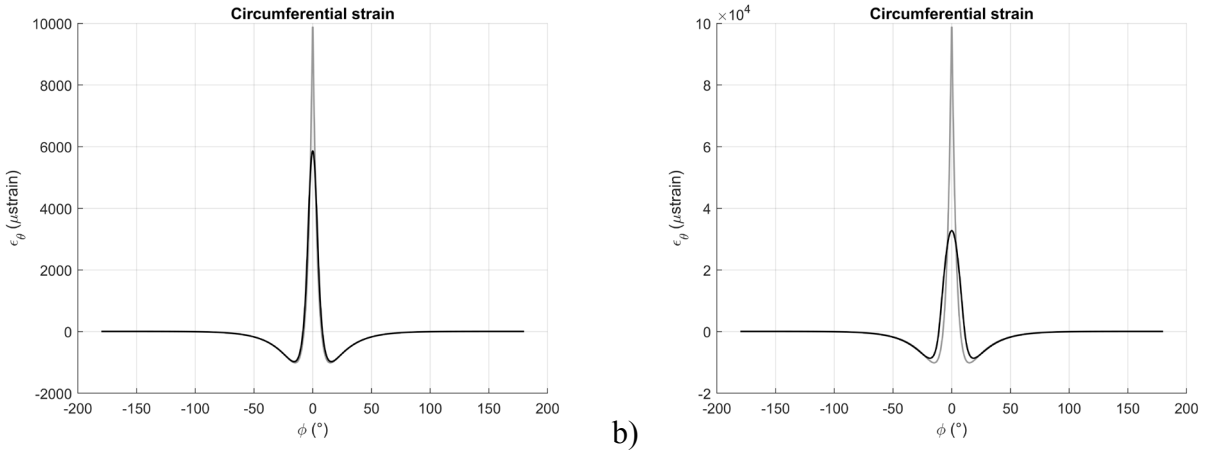

a) b)

Fig. 5. Circumferential strain: a) F_z = 500 N; b) F_z = 5000 N.

Results highlight that, for small vertical loads, the values of both radial and tangential displacements are nearly the same for the two approaches. However, it must be noted that circumferential strains do not coincide; instead, strains related to the concentrated force model are

significantly greater. At higher vertical loads, results do not coincide anymore. Of course, this phenomenon is related to the approximation adopted in assigning a concentrated force rather than a distributed pressure. While the trends of radial and tangential displacements are still comparable, with reference to the circumferential strains, the difference is almost one order of magnitude. This is in accordance with results observed also in the previous case. In any case, it is reasonable to expect that by assigning a distributed pressure trend the results are more reliable. This can be deduced from the deformed shapes of the tire, as shown in Figs. 6a,b: while the concentrated force produces a cusp which is uncharacteristic of the simple tire-road normal interaction, the response to a distributed pressure highlights the typical flat trend of the deformation in the contact patch.

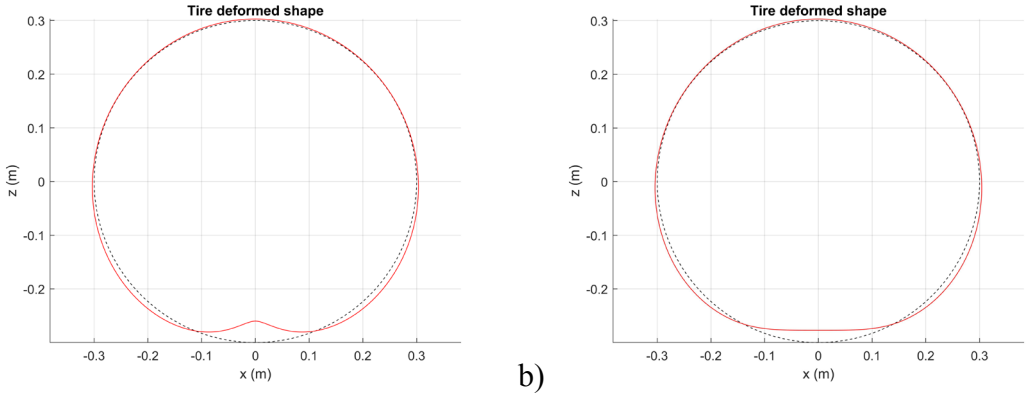

a) b)

Fig. 6: Tire deformed shape (*Fz* = 5000 N): a) Concentrated force model; b) Distributed force model.

More specifically, the response of the rolling tire to the longitudinal interaction has been investigated with the FRTM for a constant assigned vertical load F_z = 3000 N under different slip ratio conditions.

Fig. 7 shows the trend of the tangential pressure along the angular coordinate: starting from the front angle ϕ_f, τ_x grows linearly until the static friction parabola is intercepted; from this point, the trend follows that of the dynamic friction parabola (actually, even though a parabolic trend has been chosen, any normal pressure distribution could be used).

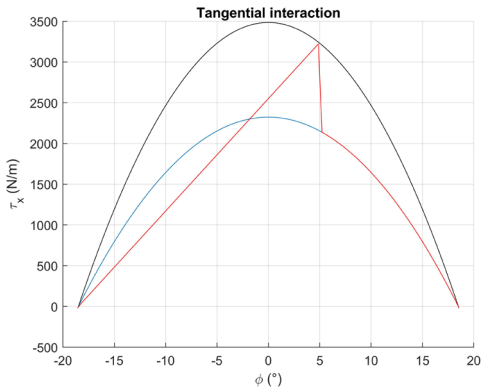

Fig. 7. Tangential pressure; (F_z = 3000 N, ε_x= -0.15).

From Figs. 8a, b the asymmetric effect of the longitudinal force on the tire deformations can be seen. Also, larger radial deformation is observed after the contact due to the longitudinal interactions of the bristles.

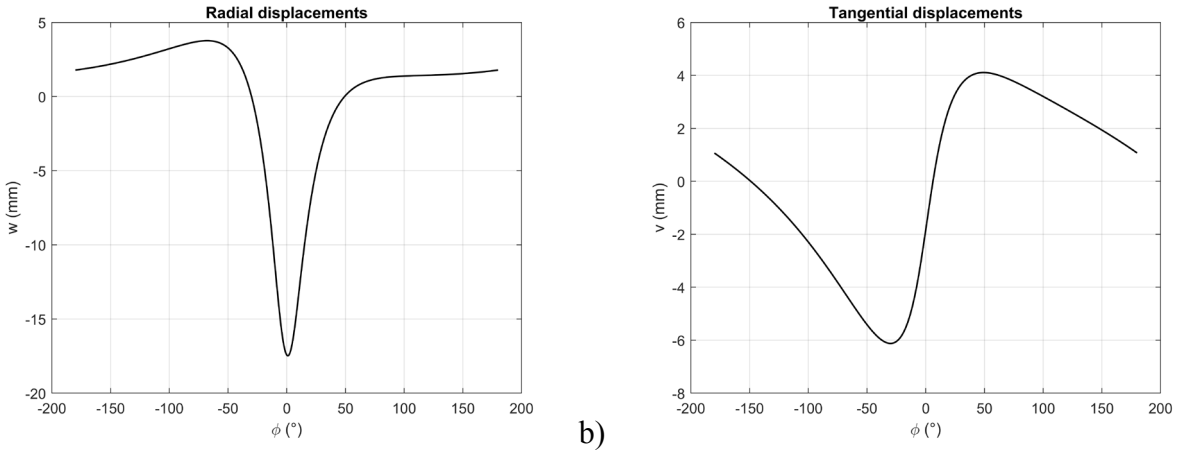

a) b)

Fig. 8. a) Radial displacements; b) Tangential displacements; (F_z = 3000, ε_x= -0.15).

The circumferential strain behaviour is shown in Fig. 9.

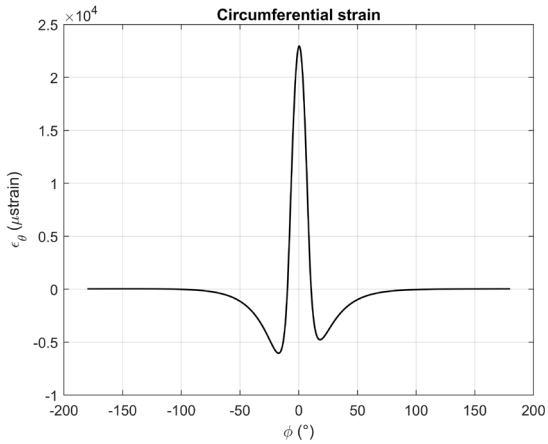

Fig. 9. Circumferential strain; (F_z = 3000, ε_x= -0.15).

The required time-step, used in the MATLAB environment, for the calculation of all the three software outputs: w, v and ε_θ is 0.01 s (angular steps =100; number of modes: 30). These values could be further reduced with a software optimization.

4. Experimental tests

To validate the FRTM, two different intelligent tires have been considered in this study. For each type of intelligent tire, the parameters have been estimated using optimization algorithms (the objective function is the root mean square error between the measured and simulated signals).

4.1. Strain-based intelligent tire [30].

At first, simulation results have been compared with real deformations measured for a strain-based intelligent tire prototype (called in the following INT1) developed in the Vehicle Dynamics Laboratory at the University of Birmingham. The pneumatic tire has been equipped with strain gauges on its inner liner [30]. Details of the intelligent tire system are shown in Fig. 10a.
The test system used for the experiments is an indoor tire test rig which makes it possible to vary speed, vertical load and slip angle. The tire test rig also allows for simulation of different surface types by installing rough sheets on the drum. The experiment setup is shown in Fig. 10b.

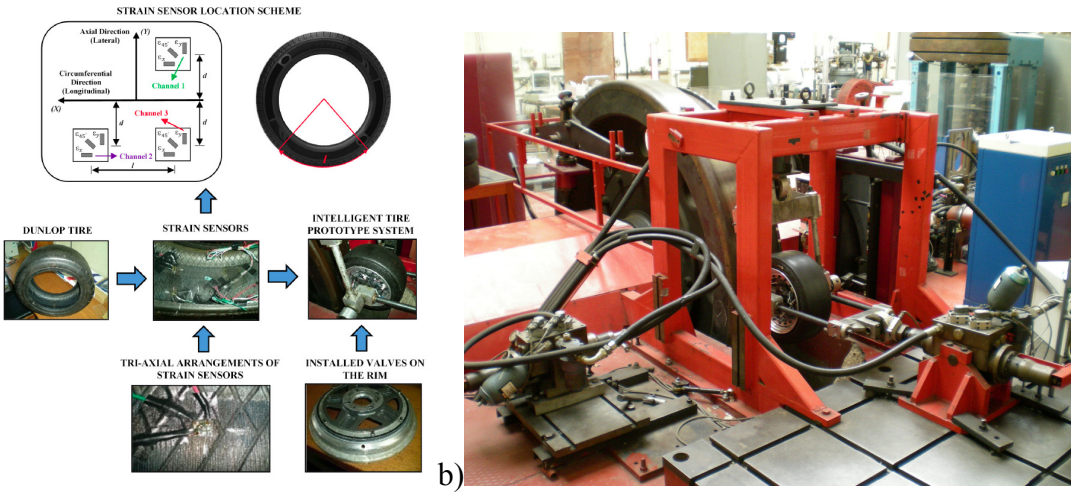

a) b)

Fig. 10. a) Strain-based intelligent tire system; b) Test rig.

The experimental data selected for the model validation are only the circumferential strains. The results have been obtained with the tire in straight-line free rolling conditions. In particular, the

influences of the tire speed and the vertical load have been evaluated (tire inflation pressure: 1 bar, tires slip angle: 0°). The simulation results have been obtained with the distributed force model reproducing a tire loading condition similar to the real one.

Fig. 11 shows the comparison between experimental and numerical results for the same tire rolling velocity of 10 km/h and a vertical load equal to 500 N. A magnification of the strains near the peak is also shown in Fig. 11.

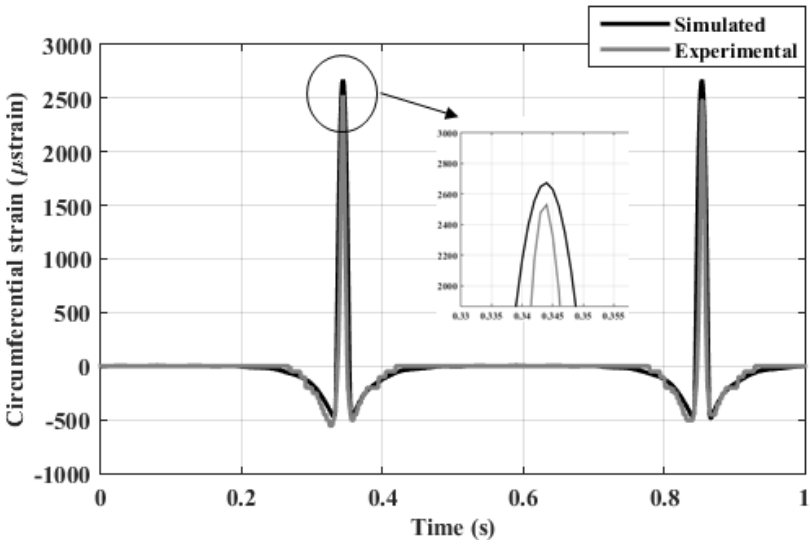

Fig. 11. a) Circumferential strain (velocity: 10 km/h; Vertical load: 500 N).

The experimental and the simulated circumferential strains for higher values of tire rolling velocity and vertical load (30 km/h and 1000 N) are presented in Fig. 12.

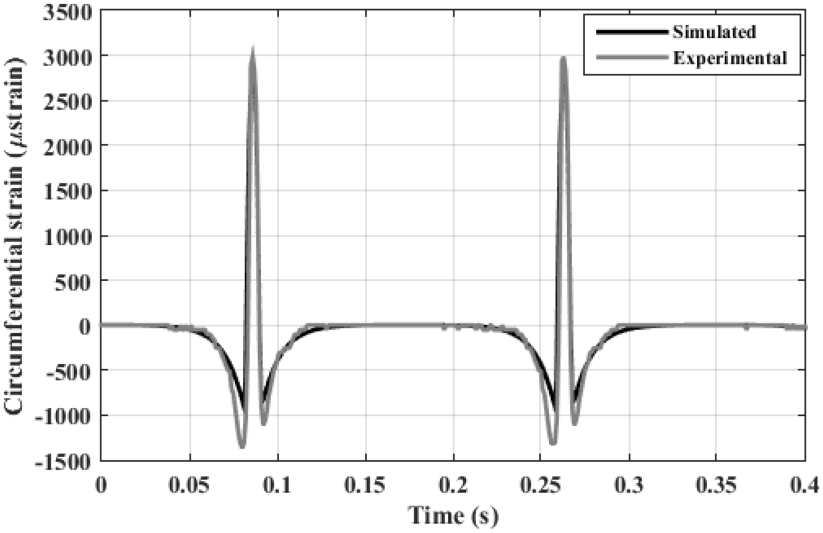

Fig. 12. Circumferential strain (velocity: 30 km/h; Vertical load: 1000 N).

The behaviours of the simulated strains for both the validation tests are in good agreement with the experimental data. In particular, the FRTM can predict the typical shape of the circumferential strain characterized by a compression in the neighbourhood of the contact patch and a maximum strain value in the middle of the contact area. Fig. 13 shows the simulated deformed shape of the tire.

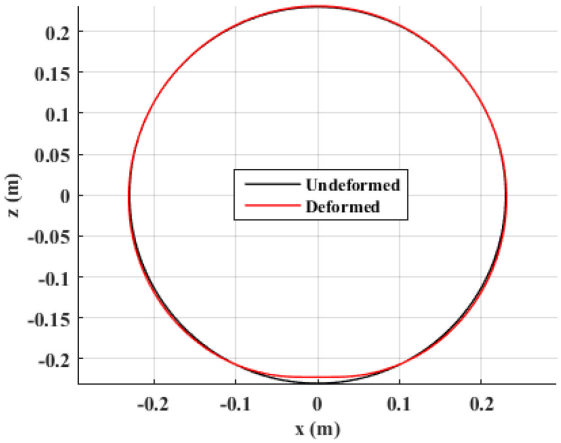

Fig. 13. Estimated tire carcass contours for the INT1 (velocity: 30 km/h; Vertical load: 1000 N).

The identified FRTM parameters for the INT1 are reported in Table 3.

Parameters	Value	Unit
b	0.175	m
h	0.002	m
EI	0.03	Nm^2
R	0.23	m
ρ	2000	kg/m
k_w	$5 \cdot 10^5$	N/m^2
k_v	$1 \cdot 10^5$	N/m^2
$c_w = c_v$	0	$N\ s/m^2$

Table 3. Identified FRTM parameters for the INT1.

One of the primary purposes of strain-based intelligent tires is the estimation of the contact patch dimensions and the lowering of the rim, since they are closely related to the maximum values of the slip parameters and to the tire/road contact forces. Detailed data about the contact patch length can be inferred from the measurements carried out on the tire treadband in circumferential and

tangential directions. The size and the shape of the contact patch vary as both the vertical and tangential loads change; however, since the proposed model is two-dimensional, only the effects of the vertical force are analysed in this paper.

4.2. Laser-based tire sensor system [17]

The second set of experimental data for the FRTM validation has been obtained by measuring the deformation of the carcass from another intelligent tire (called in the following INT2) under different in-plane forces. Data has been acquired by an optical tire sensor developed in the vehicle engineering group at Aalto University. As shown in Fig. 14a, the sensor rotates together with the rim and consists of a one-dimensional laser triangulation system which measures the distance Z from the rim to the inner liner. The instrumented tire has been tested on a tire test rig shown in Fig. 14b. The drum has been covered with safety walk paper. Three tire forces and three moments can be logged by the force sensors. The wheel load has been regulated by a controlled hydraulic system. In addition, a hydraulic disc brake system has been adopted to generate various braking forces in the longitudinal direction, which were measured by the force sensors. The camber and slip angles have been fixed to 0° to limit this study to in-plane tire deformations.

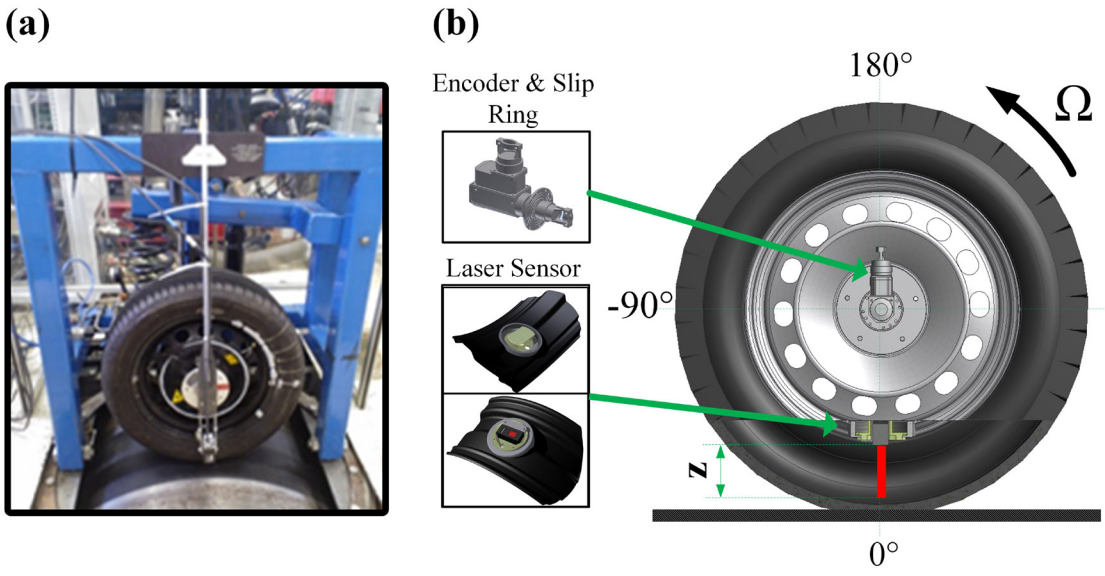

Fig. 14. a) Prototype of the laser-based tire sensor system; b) Tire test facility.

The first tests used for the model validation are related to the INT2 behaviour under vertical forces. Fig. 15 and Fig. 16 show the comparison between the treadband radial displacement from the

FRTM and the tire radial deformation measured by the laser for a vertical load of 1000 N and 5000 N, respectively (inflation pressure: 2.6 bar).

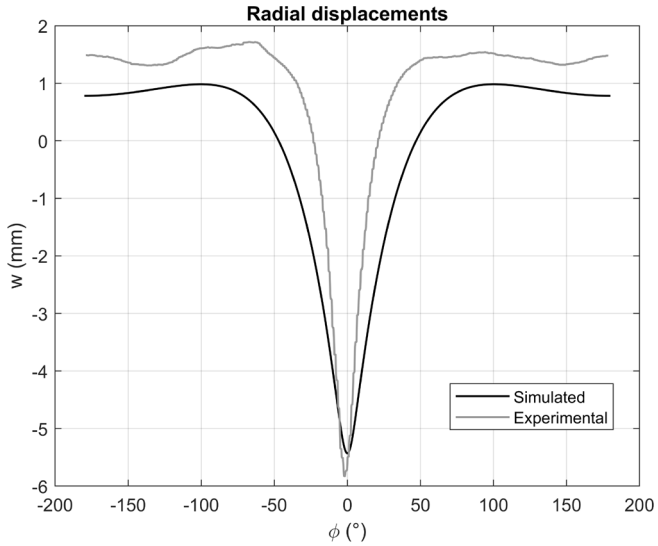

Fig. 15. Radial deformations of the INT2 (F_z = 1000 N).

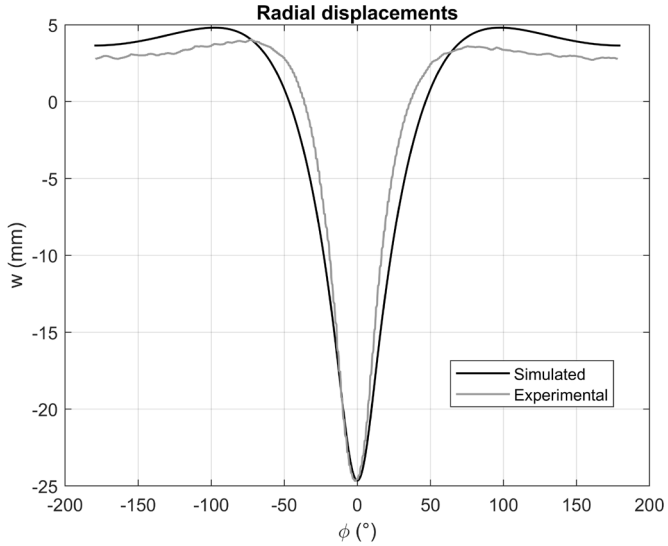

Fig. 16. Radial deformations of the INT2 (F_z = 5000 N).

Also for the INT2, the developed model is capable of reproducing the experimental deformations of the tire carcass with a good precision.

More specifically, as regards the extension of the contact patch and the normal pressure distribution, the parabolic trend gives a good approximation of the actual distributed vertical load mainly for intermediate values of the normal force and at higher levels of the inflation pressure; in contrast, at

the lower values, the trend significantly diverges and, especially with regard to small vertical loads, the length of the contact patch seems to be misestimated. However, in the examined load range, the results are generally realistic and characterized by an acceptable approximation. Therefore, the parabolic trend has also been preferred for the study of tangential interactions, since it allows to obtain accurate results in shorter times.

Further experimental data adopted for the FRTM validation in accordance with the INT2 have been obtained by applying braking longitudinal forces. Fig. 17 and Fig. 18 compare the simulated radial displacements and the measured ones, for a fixed vertical load (F_z=3000 N), a fixed inflation pressure (2.6 bar) and for longitudinal forces of 510 N and 1285 N, respectively.

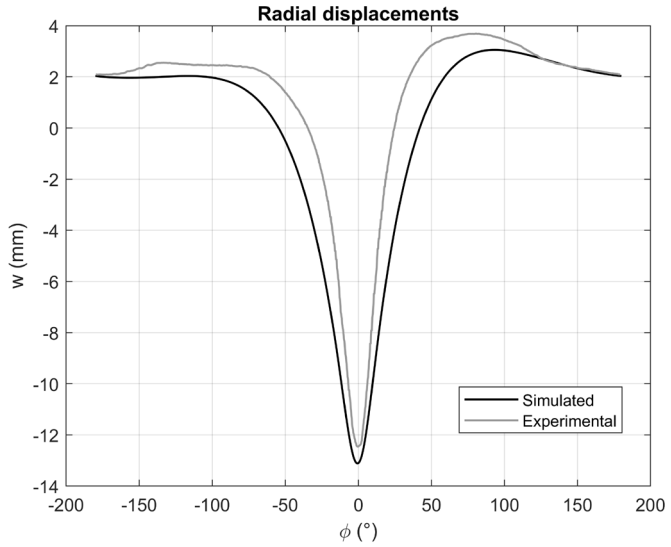

Fig. 17. Radial displacements, (F_x = 510 N, ε_x = 0.11).

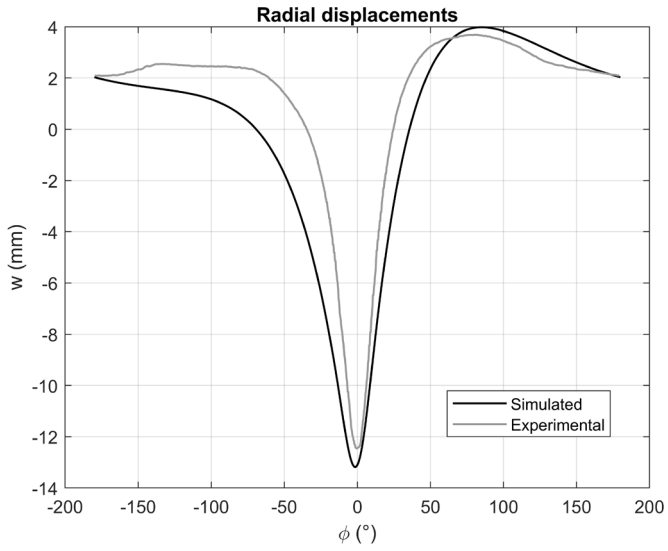

Fig. 18. Radial displacements, (F_x = 1285 N, ε_x = 0.16).

The symmetry of the radial deformation of the tire changes with the longitudinal force that is applied as a result of the pretension force and inextensibility of the ring structure. Furthermore, the maximum deformation tends to shift in the direction of the braking force.

The identified FRTM parameters for the INT2 are reported in Table 4.

Parameters	**Value**	**Unit**
b	0.16	m
h	0.001	m
EI	1.41	Nm^2
R	0.285	m
ρ	2280	kg/m
k_w	$4.88 \cdot 10^5$	N/m^2
k_v	$3.20 \cdot 10^5$	N/m^2
$c_w = c_v$	0	$N\ s/m^2$
k_x	$7.2 \cdot 10^5$	N/m

Table 4. Identified FRTM parameters for the INT2.

The displacement trends provided by the FRTM and depicted in Figs. 17-18 generally show a good agreement with the experimental ones and can be used to predict useful information such as the forces and torques applied to the wheel. More specifically, some derivative quantities of the circumferential strain have been widely employed by several authors to estimate the tire working

conditions. The commonest methods are mainly based on curve-fitting techniques for the tangential forces with high-order polynomial regression equations.

Some of these algorithms have the merit of being easily applicable and usable in a large variety of situations, but they are not generally able to properly describe in an accurate way all the phenomena arising in the contact patch. This can inevitably result in a loss of information about the physics of the problem, with a consequent difficulty in interpreting the data and with the need to correct the outputs in some circumstances.

In contrast, a full-analytical tire model capable of matching the experimental results in real-time can be extremely useful since it provides a deeper understanding of the problem's physics.

5. Observations on sensorised tire systems

The holy grail of the intelligent tire is real-time determination of the tire/road forces and deformation of the tire. Although a lot of progress has been made in this direction, there is still a lot of development required to reach this goal. A major problem is the pre-calibration required for each tire to determine the deformation and contact force characteristics under different operating conditions before the developed algorithms can be applied. Experimental tests can be used for this but the huge cost of performing a large number of tests can be prohibitive. Finite Element Analysis (FEA) is an alternative method but can also be expensive. The FRTM described in this work can be used as a much cheaper alternative to FEA for the pre-calibration. Since the model is also applicable in real-time, it can be implemented in the design of observers for real-time tire condition estimations from strain measurements.

6. Conclusions

A physical-analytical model suitable to describe the behaviour of both tire deformations and acting forces has been presented. The tire has been modelled with a flexible ring on a viscoelastic foundation. With the modal expansion method, solutions for displacements of the tire carcass and circumferential strains have been obtained in a closed-form; the discrete approach to the forces modelling has also provided physical results for both the values of normal and longitudinal loads acting on the tire.

Finally, the model has been validated by comparing simulation results with experimental data from indoor tests performed on two intelligent tires. More specifically, the first intelligent tire is equipped with strain sensors on its inner liner and the second one adopts a laser sensor system, fixed on the rotating wheel, that provides measurements of the tire carcass deformation.

Analyses carried out confirm the high performance of the proposed approach, which could be used for predicting the dynamical behaviour of both the strain-based intelligent tire and the laser-based one. It may also be used in the design of real-time observers for tire condition based on tire strain measurements.

References

[1] Lee, H., Taheri, S. Intelligent tires-a review of tire characterization literature (2017) IEEE Intelligent Transportation Systems Magazine, 9 (2), art. no. 7904765, pp. 114-135.

[2] Singh, K.; Bedekar, V.; Taheri, S.; Priya, S. Piezoelectric vibration energy harvesting system with an adaptive frequency tuning mechanism for intelligent tires. Mechatronics 2012, 22, 970–988.

[3] Negrus, E.; Anghelache, G.; Sorohan, S. Tire Radial Vibrations at High Speed of Rolling; SAE: Detroit, MI, USA, 1998.

[4] Hong, S.; Erdogan, G.; Hedrick, K.; Borrelli, F. Tyre–road friction coefficient estimation based on tyre sensorsand lateral tyre deflection: Modelling, simulations and experiments. Veh. Syst. Dyn. 2013, 51, 627–647.

[5] F. Braghin, M. Brusarosco, F. Cheli, A. Cigada, S. Manzoni, and F. Mancosu, "Measurement of contact forces and patch features by means of accelerometers fixed inside the tire to improve future car active control," Vehicle Syst. Dyn., vol. 44, no. 1, pp. 3–13, Jan. 2006.

[6] K. S. Moona, H. Liangb, J. Yi, and B. Mika, "Tire tread deformation sensor and energy harvester development for "Smart Tire" applications," in Proc. Sensors and Smart Structures Technologies for Civil, Mechanical, and Aerospace System, San Diego, CA, 2007.

[7] J. Yi, "A piezo-sensor-based 'smart tire' system for mobile robots and vehicles," IEEE/ASME Trans. Mechatron., vol. 13, no. 1, pp. 95–103, Feb. 2008.

[8] A. Pohl, R. Steindl, and L. Reindl, "The 'intelligent tire' utilizing passive SAW sensors measurement of tire friction," IEEE Trans. Instrum. Meas., vol. 48, no. 6, pp. 1041–1046, 1999.

[9] A. Todoroki, S. Miyatani, and Y. Shimamura, "Wireless strain monitoring using electrical capacitance change of tire: Part I—with oscillating circuit," Smart Mater. Struct., vol. 12, no. 3, pp. 403–409, May 2003.

[10] O. Yilmazoglu, M. Brandt, J. Sigmund, E. Genc, and H. L. Hartnagel, "Integrated InAs/GaSb 3D magnetic field sensors for 'the intelligent tire," Sens. Actuators A, vol. 94, no. 1/2, pp. 59–63, Oct. 2001.

[11] A. Miyoshi, T. Tsurita, and M. Kunni, "System and method for determining tire force," U.S. Patent 7 249 498, July 31, 2007.

[12] N. Roveri, G. Pepe, A. Carcaterra, "OPTYRE – A new technology for tire monitoring: Evidence of contact patch phenomena," Mechanical Systems and Signal Processing, vol. 66–67, pp. 793-810, 2016.

[13] Breglio, G., Fienga, F., Irace, A., Russo, M., Strano, S., Terzo, M. Fiber Bragg gratings for strain and temperature measurements in a smart tire (2017) Lecture Notes in Engineering and Computer Science, 2230, pp. 759-763.

[14] Garcia-Pozuelo, D., Yunta, J., Olatunbosun, O., Yang, X., Diaz, V. A strain-based method to estimate slip angle and tire working conditions for intelligent tires using fuzzy logic (2017) Sensors (Switzerland), 17 (4), art. no. 874.

[15] Garcia-Pozuelo, D., Olatunbosun, O., Yunta, J., Yang, X., Diaz, V. A novel strain-based method to estimate tire conditions using fuzzy logic for intelligent tires (2017) Sensors (Switzerland), 17 (2), art. no. 350.

[16] Magori, V.; Magori, V.R.; Seitz, N. On-Line Determination of. Tire Deformation, a Novel Sensor Principle. In Proceedings of the IEEE Ultrasonics Symposium, Sendai, Japan, 5–8 October 1998.

[17] Tuononen, A. Optical position detection to measure tyre carcass deflections. Veh. Syst. Dyn. 2008, 46, 471–481.

[18] Tuononen, A. Optical Position Detection to Measure Tire Carcass Deflections and Implementation for Vehicle State Estimation. Ph.D. Thesis, Helsinki University of Technology, Espoo, Finland, 2009.

[19] Cullen, J.; Arvanitis, N.; Lucas, J.; Al-Shamma'a, A. In-field trials of a tyre pressure monitoring system based on segmented capacitance rings. Measurement 2002, 32, 181–192.

[20] Canudas de Wit, C. and Tsiotras, P. (1999). Dynamic tire friction models for vehicle traction control. Proc. 38th Conf. Decision & Control, 4, 3746−3751.

[21] Rajamani, R. (2012). Vehicle Dynamics and Control. 2nd edn. Springer. New York.

[22] Jazar, R. N. (2008). Vehicle Dynamics: Theory and Application. Springer. New York.

[23] Tonuk, E. and Unlusoy, Y. S. (2001). Prediction of automobile tire cornering force characteristics by finite element modeling and analysis. Computers & Structure 79, 13, 1219−1232.

[24] Lee, C. R., Kim, J. W., Hallquist, J. O., Zhang, Y. and Farahani, A. D. (1997). Validation of a FEA tire model for vehicle dynamic analysis and full vehicle real time proving ground simulations. SAE Paper No. 971100.

[25] Yang, X.; Olatunbosun, O.; Garcia-Pozuelo Ramos, D.; Bolarinwa, E. FE-Based Tire Loading Estimation for Developing Strain-Based Intelligent Tire System; SAE: Detroit, MI, USA, 2015.

[26] Holtschulze, J., Goertz, H. and Husemann, T. (2005). A simplified tyre model for intelligent tyres. Vehicle System Dynamics, 43, 305−316.

[27] S. Gong, A Study of In-Plane Dynamics of Tires, Delft University, 1993.

[28] Kim, Son-Joo, Savkoor, Arvin R. Contact problem of in-plane rolling of tires on a flat road (1997) Vehicle System Dynamics, 27 (Suppl), 345 p.

[29] Xiong, Y., Tuononen, A. The in-plane deformation of a tire carcass: Analysis and measurement (2015) Case Studies in Mechanical Systems and Signal Processing, 2, pp. 12-18.

[30] Yang X. Finite element analysis and experimental investigation of tyre characteristics for developing strain-based intelligent tyre system. In Mechanical engineering. Birmingham: University of Birmingham; 2009.

[31] Zegelaar, Peter W.A; The Dynamic Response of Tyres to Brake Torque Variations and Road Unevennesses, Delft University, 1998.

[32] Seongho Kim, Parviz E. Nikravesh & Gwanghun Gim (2008) A two-dimensional tire model on uneven roads for vehicle dynamic simulation, Vehicle System Dynamics, 46:10, 913:930, DOI: 10.1080/00423110701729994

[33] G. Mastinu, S. Gaiazzi, F. Montanaro & D. Pirola (1997) A Semi-Analytical Model for Steady- and Transient-State Simulations, Vehicle System Dynamics, 27:S1, 2-21, DOI: 10.1080/00423119708969641